Forced-Oscillation Test Mechanism for Measuring Dynamic-Stability Derivatives in Roll

Glen E. Burt*
ARO, Inc., Arnold Air Force Station, Tenn.

A description of a test mechanism and associated instrumentation for measuring rolling moment, yawing moment, and side force due to roll velocity on lifting configurations is presented. Models with a cavity diameter of two inches can be installed on the water-cooled test mechanism which can support 1200 lb normal force and 300 lb axial force. Results of bench tests and wind tunnel verification tests on an AGARD Model-B indicate the system can accurately measure dynamic moments of 0.05 in.-lb. In addition to the dynamic measurements, the system simultaneously obtains five-component static-force and moment data.

Nomenclature

A = reference area, model wing area, 0.974 ft^2
b = reference length for lateral coefficients, wing span, 1.500 ft
C_l = rolling-moment coefficient, $L/q_\infty Ab$
C_{l_p} = rolling-moment coefficient due to roll velocity $\partial(C_l)/\partial(pb/2V_\infty)$, rad^{-1}
C_{l_β} = rolling-moment coefficient due to sideslip angle, $\partial(C_l)/\partial\beta$, rad^{-1}
$C_{l_{\dot\beta}}$ = rolling-moment coefficient due to rate of change of sideslip angle, $\partial(C_l)/\partial(\dot\beta b/2V_\infty)$, rad^{-1}
C_m = pitching-moment coefficient, $M/q_\infty Ac$
C_N = normal-force coefficient, Normal Force$/q_\infty A$
C_n = yawing-moment coefficient, $N/q_\infty Ab$
C_{n_p} = yawing-moment coefficient due to roll rate, $\partial(C_n)/\partial(pb/2V_\infty)$, rad^{-1}
$C_{n_{\dot\beta}}$ = yawing-moment coefficient due to rate of change of sideslip angle, $\partial(C_n)/\partial(\dot\beta b/2V_\infty)$, rad^{-1}
C_Y = side-force coefficient, $Y/q_\infty A$
$C_{Y_{\dot\beta}}$ = side-force coefficient due to rate of change of sideslip angle, $\partial(C_Y)/\partial(\dot\beta b/2V_\infty)$, rad^{-1}
C_{Y_p} = side-force coefficient due to roll velocity, $\partial(C_Y)/\partial(pb/2V_\infty)$, rad^{-1}
c = reference length for longitudinal coefficients, wing mean aerodynamic chord, 0.866 ft
I_X = model moment of inertia about the x-axis, slug-ft^2
I_{xz} = product of inertia about the x- and z-axes, slug-ft^2
I_z = model moment of inertia about the z-axis, slug-ft^2
K_0 = flexure calibration constant, rad/v
K_1, K_2 = balance forward and aft pitching-moment calibration constants, ft-lb/v
K_3, K_4 = balance forward and aft yawing-moment calibration constants, ft-lb/v
K_5 = balance rolling-moment calibration constant, ft-lb/v
L = moment about the model x axis (rolling moment), ft-lb
L_b = input torque in roll, ft-lb
L_β = rolling moment due to sideslip angle, $\partial L/\partial\beta$, ft-lb/rad
$L_{\dot\beta}$ = rolling moment due to rate of change of sideslip angle, $\partial L/\partial\dot\beta$, ft-lb-sec/rad
L_ϕ = rolling moment due to roll angle, $\partial L/\partial\phi$, ft-lb/rad
$L_{\dot\phi}$ = rolling moment due to rate of change of roll angle, $\partial L/\partial\dot\phi$, ft-lb-sec/rad
M = moment about the model y-axis (pitching-moment), ft-lb
M_∞ = freestream Mach number
N = moment about the model z-axis (yawing-moment), ft-lb
N_β = yawing moment due to sideslip angle, $\partial N/\partial\beta$, ft-lb/rad
$N_{\dot\beta}$ = yawing moment due to rate of change of sideslip angle, $\partial N/\partial\dot\beta$
N = yawing moment due to rate of change of roll angle, $\partial N/\partial\dot\phi$, ft-lb-sec/rad
N_ψ = yawing moment due to yaw angle, $\partial N/\partial\psi$, ft-lb/rad
$N_{\dot\psi}$ = yawing moment due to rate of change of yaw angle, $\partial N/\partial\dot\psi$, ft-lb-sec/rad
p = rolling velocity, rad/sec
p_o = tunnel stilling chamber pressure, psia
q_∞ = tunnel freestream dynamic pressure, lb/ft^2
$Re_{\infty,c}$ = tunnel freestream Reynolds number based on c
T_o = tunnel stilling chamber temperature, °R
t = time, sec
V_∞ = tunnel freestream velocity, fps
x, y, z = body-fixed axis system
x_1, x_2 = location of forward and aft yaw strain gage electrical centers, respectively, ft
x_R = location of moment reference point, ft
Y = side force, lb
$Y_{\dot\beta}$ = side force due to rate of change of sideslip angle, $\partial Y/\partial\dot\beta$–, lb-sec/rad
$Y_{\dot\phi}$ = side force due to rate of change of roll angle, $\partial Y/\partial\dot\phi$, lb-sec/rad
α = angle of attack, deg
β = sideslip angle, rad
Γ = phase angle between yawing moment, N, and roll angle, ϕ (positive when N leads), rad
γ = phase angle between input torque, L_b, and roll angle, ϕ (positive when L_b leads), rad or deg
ϕ = angular displacement about the x-axis (roll angle), rad or deg
ψ = angular displacement about the z-axis (yaw angle), rad
ω = model angular oscillation frequency, rad/sec
ω_{n_ϕ} = model-flexure natural frequency in roll at vacuum conditions, rad/sec
ω_{n_ψ} = model-flexure natural frequency in yaw at vacuum conditions, rad/sec
$(\dot{})(\ddot{})$ = first and second derivatives with respect to time, t
$(\bar{})$ = amplitude
$\Delta()$ = probable error

Subscripts

a = aerodynamic
b = balance
f = flexure
mag = magnetic damper
r = resolvers
S = static
1 = forward balance section
2 = aft balance section

Presented as Paper 74-86 at the AIAA 12th Aerospace Sciences Meeting, Washington, D.C., January 30–February 1, 1974; submitted February 11, 1974; revision received September 6, 1974. The research reported herein was conducted by the Arnold Engineering Development Center (AEDC), Air Force Systems Command (AFSC). Research results were obtained by personnel of ARO, Inc., contract operator at AEDC. Further reproduction is authorized to satisfy needs of the U.S. Government.

Index categories: Aircraft Testing (Including Component Wind Tunnel Testing); Nonsteady Aerodynamics.

*Supervisor, Dynamics Group, Aerodynamics Projects Branch, von Kármán Gas Dynamics Facility, AEDC. Member AIAA.

I. Introduction

THE advent of high performance, supersonic military airplanes and re-entry lifting bodies such as the F-15, the B-1, and the Space Shuttle has created the requirement to develop new dynamic-stability test mechanisms for the von Kármán Gas Dynamics Facility (VKF) continuous-flow wind tunnels. To meet the requirements for large lift loads and relatively large damping moments, and to maintain compatibility with expected model configurations, the forced-oscillation technique has been selected. This paper covers the development and checkout, includ-

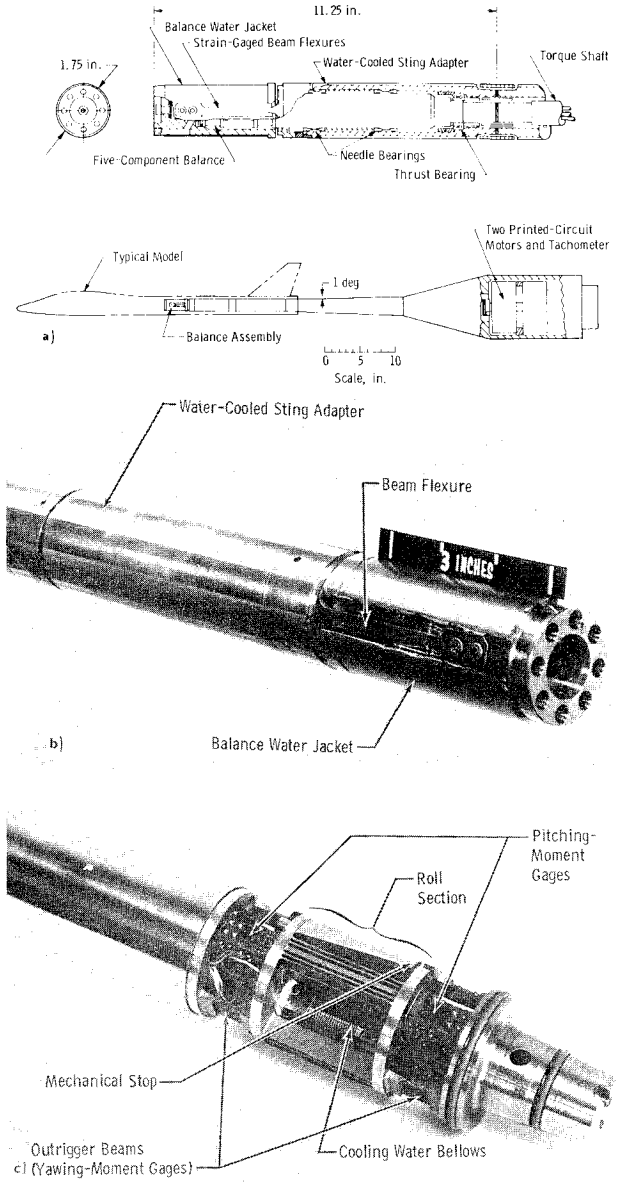

Fig. 1 Test mechanism: a) details, b) photograph of the flexures and water jacket, c) photograph of the balance.

ing wind tunnel verification testing, of a mechanism used to determine the coefficients due to roll rate (rolling moment, yawing moment, and side force) on lifting configurations. Other mechanisms and facilities used to obtain these measurements are summarized in Ref. 1. This mechanism can support models with a combined loading of up to 1200 lb of normal force and 300 lb of axial force. Although this mechanism was designed primarily to obtain dynamic measurements, the technique employed also produces five-component static force and moment data. The wind-tunnel verification tests were conducted in the VKF Supersonic Wind Tunnel (A) at Mach numbers 2, 3, and 4 on an AGARD Calibration Model B.

II. Apparatus

Test Mechanism

The VKF 1.D roll-damping test mechanism (Fig. 1) utilizes a water-jacketed, five-component balance, twin beam flexures, roller bearings to support the loads, and electric printed-circuit drive motors. The motors are directly coupled to the balance and supply up to 120 in.-lb roll moment to oscillate the system at amplitudes up to ±3° and at frequencies from 2 to 20 Hz. The twin beam flexures mount from the stationary sting to the oscillating water jacket and provide a restoring moment which cancels the inertia moment when the system is operating at the natural frequency of the model-flexure system. The flexures are instrumented to measure the roll displacement. The entire mechanism is water-cooled to permit testing in the hypersonic tunnels.

Table 1 Balance load capacity

Balance	Normal force	Pitching moment	Side force	Yawing moment	Rolling moment
−59	500 lb	1125 in.-lb	40 lb	84 in.-lb	10 in.-lb
−60	1200 lb	2700 in.-lb	100 lb	210 in.-lb	100 in.-lb

Two five-component balances have been fabricated for the system to provide good balance sensitivity over the load range. Both balances utilize outrigger beams in the yaw sections (Fig. 1c) and thin-ribbed flexures in the roll section to provide sensitive yaw and roll outputs while maintaining large normal-force capacity and rigidity in yaw. Semiconductor gages are also utilized for the yaw and roll sections for additional sensitivity. The load capacity of the two balances is listed in Table I.

Instrumentation

The forced-oscillation instrumentation described in Ref. 2 was modified to improve the control and monitor systems and thereby to provide more accurate data with less computer time required. These changes were made by using an electronic analog system with precision electronics. The control, monitor, and data acquisition instrumentation is contained in a portable console that can be easily interfaced with the instrumentation of the various wind tunnels.

The control instrumentation provides a system which can vary the oscillation frequency, oscillation amplitude, and roll position of the model within the flexure limits. The oscillation amplitude is controlled by an electronic feedback loop which permits testing both dynamically stable and unstable configurations.

Data are normally obtained at or near the natural frequency of the model-flexure system; however, the electronic resolvers used permit data to be obtained off resonance. A schematic of the data acquisition system is shown in Fig. 2. The gages on the balance and flexures are excited by d.c. voltages, and outputs are increased to optimum values by d.c. amplifiers. Typical balance and flexure outputs from an oscillating model are composed of oscillatory components (OC) superimposed on static components (SC). These components are separated in the data system by bandpass and lowpass filters. The SC outputs are sent directly to the tunnel scanner and computer, which calculate the static-force and moment coefficients, C_N, C_m, C_Y, C_n, and C_l. The OC outputs are input to the resolver instrumentation (Fig. 2b) and the precise frequency-measuring instrument which were developed at VKF. The resolvers utilize very accurate analog electronic devices to process the OC signals and output d.c. voltages, which are proportional to the amplitude squared, the in-phase and quadrature (90° out of phase) rolling moments, and the quadrature yawing moments. A switch is also provided in the resolver system to bypass the phase shift network so that the in-phase yawing moments can be determined. The resolver and frequency outputs are read by the tunnel scanner and sent to the computer. The frequency instrument controls the length of the data interval in increments from approximately 2 to 25 sec, during

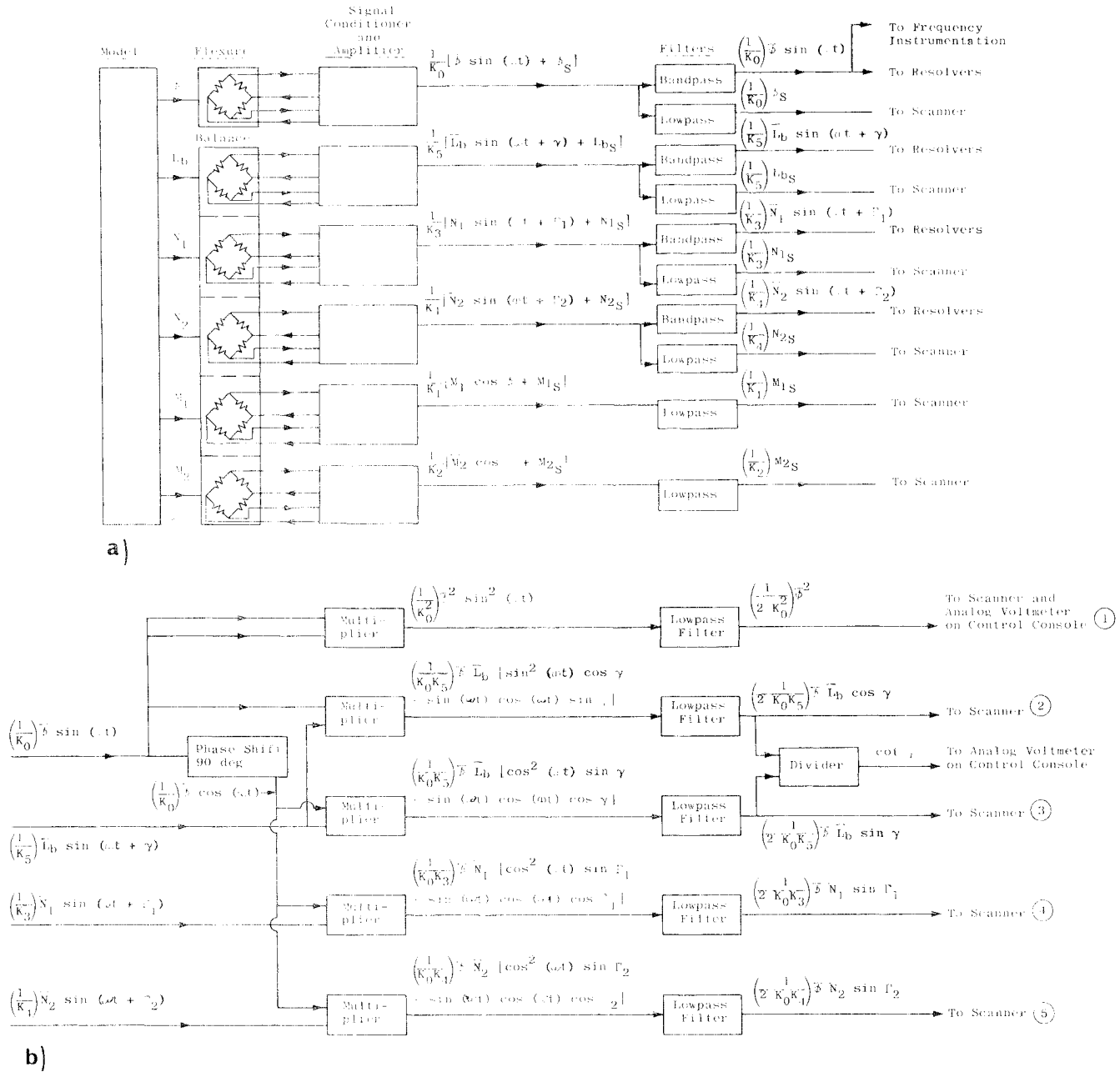

Fig. 2 Data acquisition instrumentation schematic: a) balance outputs, b) resolver system.

which time the scanner reads each input approximately 10 times per second. The average values of the readings are calculated by the computer, which then uses these average values to calculate the dynamic coefficients $C_{l(p)} + C_{l(\dot{\beta})} \sin \alpha$, $C_{n(p)} + C_{n(\dot{\beta})} \sin \alpha$, and $C_{Y(p)} + C_{Y(\dot{\beta})} \sin \alpha$ as described in Sec. III-A.

Model

The model used for the wind tunnel verification testing was a 4.5-in.-diam AGARD Calibration Model B (Fig. 3) which was obtained on loan from the Cornell Aeronautical Laboratory. The body is a tangent ogive cylinder with a fineness ratio of 8.5. The 60° delta wing has a symmetrical, circular-arc cross section with a thickness ratio of 0.04 and a span of four body diameters. The model was constructed primarily of aluminum but contained some steel for additional strength at the wing mounting location. The model was mounted to the test mechanism in such a way that there was a distance of nearly 4.5 body diameters from the model base to the sting flare.

Wind Tunnel

Tunnel A is a continuous, closed-circuit, variable density wind tunnel with an automatically driven flexible-plate-type nozzle and a 40- by 40-in. test section. The tunnel can be operated at Mach numbers from 1.5 to 6 at maximum stagnation pressures from 29 to 200 psia, respectively, and stagnation temperatures up to 750°R (at $M_\infty = 6$). Minimum operating pressures range from about one-tenth to one-twentieth of the maximum pressure at each Mach number. In most instances, Mach number changes may be made without stopping the tunnel. The model can be injected into the tunnel for a test run and then retracted for model changes without stopping the tunnel flow.

III. Procedure

A. Data Reduction

The test mechanism operates basically as a one-degree-of-freedom system in roll (body axis system); however, it

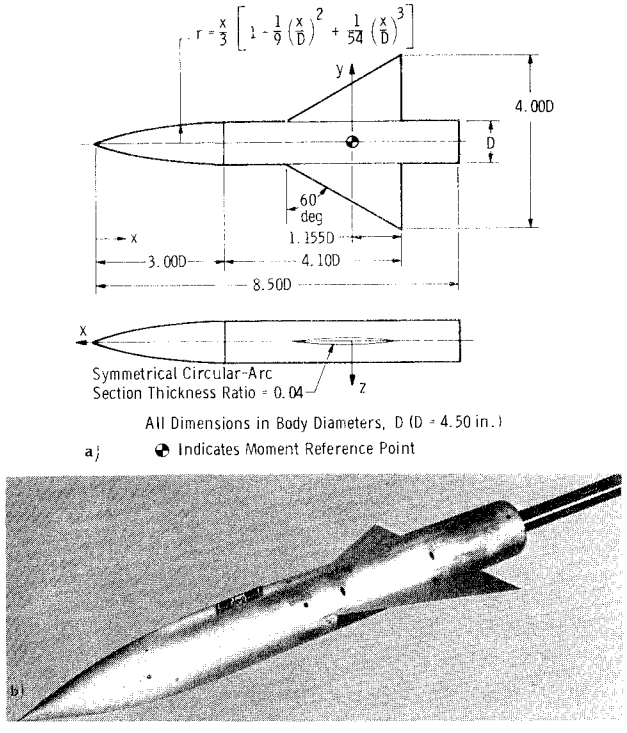

Fig. 3 Model description: a) details, b) installation photograph.

is obvious that for the balance to measure the dynamic yawing moments it must also deflect in yaw. Therefore, both the roll and yaw equations of motion must be considered. The equations can be simplified considerably if the balance is made very stiff in the yaw direction and the system is not operated near the natural yaw frequency ($\omega_{n(\psi)} > 1.5\omega$). With these conditions it is assumed that

$$\sin\phi = \phi$$
$$\bar{\psi} << \bar{\phi}$$
$$N_{\dot{\psi}b} >> N_{\dot{\psi}a}$$
$$N_{\dot{\psi}}\dot{\psi} = 0$$
$$\phi \sin\alpha \approx \beta$$

Now the roll equation of motion can be written

$$I_x\ddot{\phi} - (L_{\dot{\phi}_a} + L_{\dot{\beta}_a}\sin\alpha + L_{\dot{\phi}_f}^{\cdot})\dot{\phi} - (L_{\beta_a}\sin\alpha + L_{\phi_f})\phi = L_b \quad (1)$$

which is independent of yaw. The yaw equation of motion can be written

$$I_z\ddot{\psi} + I_{xz}\ddot{\phi} - (N_{\dot{\phi}}^{\cdot} + N_{\dot{\beta}}^{\cdot}\sin\alpha + N_{\dot{\phi}_f}^{\cdot})\dot{\phi} - N_\beta\sin\alpha\phi = N_{\psi_b}\psi \quad (2)$$

The solution of these equations for a system oscillating at a steady-state condition at some amplitude, $\bar{\phi}$, may be written

$$\phi = \bar{\phi}\cos\omega t$$
$$L_b = \bar{L}_b\cos(\omega t + \gamma) \quad (3)$$
$$\psi = \bar{\psi}\cos(\omega t + \Gamma)$$

Now substituting in the roll equation gives

$$(L_{\dot{\phi}}^{\cdot} + L_{\dot{\beta}}^{\cdot}\sin\alpha)_a = \left(-\frac{\bar{L}_b}{\bar{\phi}}\sin\gamma - L_{\dot{\phi}_f}^{\cdot}\omega\right)\frac{1}{\omega} \quad (4)$$

and

$$(L_\beta\sin\alpha)_a = -\frac{\bar{L}_b}{\bar{\phi}}\cos\gamma + L_{\phi_f}\left[\left(\frac{\omega}{\omega_{n_\phi}}\right)^2 - 1\right] \quad (5)$$

where $-L_{\phi(f)}/(\omega_{n(\phi)})^2$ has been substituted for I_x. The terms $(\bar{L}_b/\bar{\phi})\sin\gamma$ and $(\bar{L}_b/\bar{\phi})\cos\gamma$ can be obtained directly from the resolvers (Fig. 2b) by dividing outputs 3 and 2, respectively, by output 1 and the appropriate balance calibration factors. $L_{\phi(f)}$ is determined in the flexure-balance calibration, and $L_{\phi(f)}$ and $\omega_{n(\phi)}$ can be obtained by evaluating the system at vacuum conditions in a manner similar to that discussed for pitch in Ref. 2. The damping of the beam flexure, $L_{\dot{\phi}(f)}$, varies inversely with frequency (i.e., $L_{\dot{\phi}(f)}\omega$ is constant), which is the same result found for cross flexures in Ref. 3.

Now substituting Eqs. (3) in the yaw equation of motion [Eq. (2)] and taking the quadrature (i.e., $\sin\omega t$) terms gives

$$(N_{\dot{\phi}}^{\cdot} + N_{\dot{\beta}}^{\cdot}\sin\alpha)_a = -\frac{\bar{\psi}\sin\Gamma}{\bar{\phi}\omega}[N_{\psi_b} + I_z(\omega)^2] - N_{\dot{\phi}_f}^{\cdot} \quad (6)$$

Now substituting $-N_{\psi(b)}/(\omega_{n(\psi)})^2$ for I_z and realizing $N_{\psi(b)}\psi$ is the moment measured by the balance N, Eq. (6) can be written

$$(N_{\dot{\phi}}^{\cdot} + N_{\dot{\beta}}^{\cdot}\sin\alpha)_{a_{1,2}} = -\frac{\bar{N}_{1,2}\sin\Gamma}{\bar{\phi}\omega}\left[1 - \left(\frac{\omega}{\omega_{n_\psi}}\right)^2\right] - N_{\dot{\phi}_f}^{\cdot} \quad (7)$$

where 1 and 2 denote moments obtained from forward and aft yaw sections of the balance, respectively. The terms $\bar{N}_{1,2}\sin\Gamma/\bar{\phi}$ are obtained from resolver outputs 4, 5, and 1 (Fig. 2b), $\omega_{n(\psi)}$ can be obtained by wind-off, free oscillation, and $N_{\phi(f)}$ can be obtained by evaluating the system at vacuum. The side force due to roll rate can be determined from the two yawing moments obtained from Eq. (7) as

$$(Y_{\dot{\phi}}^{\cdot} + Y_{\dot{\beta}}^{\cdot}\sin\alpha)_a = \frac{(N_{\dot{\phi}}^{\cdot} + N_{\dot{\beta}}^{\cdot}\sin\alpha)_{a_2} - (N_{\dot{\phi}}^{\cdot} + N_{\dot{\beta}}^{\cdot}\sin\alpha)_{a_1}}{x_1 - x_2} \quad (8)$$

It should be noted that although the in-phase terms of the yaw equation were not required to obtain the desired data, they can be important in two respects. First, if the product of inertia term $I_{xz}\ddot{\phi}$ is large, it produces a large yaw-forcing function which increases the yaw amplitude in such a way that the balance capacity is reached or the assumption that $\bar{\psi} \ll \bar{\phi}$ may be invalidated. Second, a portion of the in-phase terms is inherently included in the quadrature measurement because of resolver uncertainty, and thus it is desirable to minimize the in-phase term in order to get better data precision.

The parameters obtained in Eqs. (4, 5, 7, and 8) can be expressed in coefficient form as follows:

$$C_{l_p} + C_{l_{\dot{\beta}}}\sin\alpha = \frac{(L_{\dot{\phi}}^{\cdot} + L_{\dot{\beta}}^{\cdot}\sin\alpha)_a(2V_\infty)}{q_\infty Ab^2}$$

$$C_{l_\beta}\sin\alpha = \frac{(L_\beta\sin\alpha)_a}{q_\infty Ab}$$

$$C_{n_p} + C_{n_{\dot{\beta}}}\sin\alpha = \frac{[(N_{\dot{\phi}}^{\cdot} + N_{\dot{\beta}}^{\cdot}\sin\alpha)_{a_1}(x_R - x_2) - (N_{\dot{\phi}}^{\cdot} + N_{\dot{\beta}}^{\cdot}\sin\alpha)_{a_2}(x_R - x_1)]2V_\infty}{(x_1 - x_2)q_\infty Ab^2}$$

$$C_{Y_p} + C_{Y_{\dot{\beta}}}\sin\alpha = \frac{(Y_{\dot{\phi}}^{\cdot} + Y_{\dot{\beta}}^{\cdot}\sin\alpha)_a(2V_\infty)}{q_\infty Ab}$$

Table 2 Summary of test conditions

Mach no.	p_o, psia	T_o, °R	q_∞, lb/ft²	V_∞, fps	$Re_{\infty,c} \times 10^{-6}$	α, deg
2.00	19	562	979	1732	3.99	−4.5 to 10.3
3.01	32	562	784	2086	4.05	−4.4 to 11.0
3.99	10	562	107	2267	0.76	−4.3 to 10.9
4.02	55	562	575	2271	4.10	−4.3 to 10.7
4.03	72	562	746	2272	5.34	−4.1 to 10.1

In the preceding analysis the balance input torque, L_b, and yawing moment, N, signals have been assumed to be the first harmonic of the oscillation frequency, ω. Because of nonlinear aerodynamics, tunnel noise, flow perturbations, etc., these signals are often composed of higher and lower harmonics. However, the resolver system (Fig. 2b) eliminates the higher harmonics, and the lower harmonics can be eliminated by averaging the data over a sufficiently long interval.

B. Calibration and Bench Tests

A complex balance calibration was required, which involved calibration of the balance and flexures separately and then in combination to determine all the calibration constants and interaction terms. For the present balances, the interactions affecting the dynamic measurements were small and usually negligible.

Bench tests were conducted with the system to determine its capability in measuring the dynamic quantities. A VKF-developed two-arm magnetic damper was used to produce known moments and forces proportional to roll velocity. A signal coil, input coil, and feedback loop were used in such a way that both stable and unstable roll moments could be produced by changing the phasing of the input coil on both arms. By changing the phasing of the input coil on one arm only, a side force and yawing moment proportional to the roll velocity could be created. The magnitude of these forces and moments could be varied by changing the gain in the feedback loop.

C. Wind-Tunnel Tests

Tests were conducted on a 4.50-in.-diam AGARD Model B at Mach numbers 2, 3, and 4, at Reynolds numbers 0.76, 4.08, and 5.38 million, and at angles of attack from −4° to 11°. The data were obtained primarily at an oscillation amplitude, $\bar{\phi}$, of 1.2° and near the roll resonant frequency (i.e., $\gamma \approx 90°$); however, some data were obtained off resonance ($20 < \gamma < 160$) to check the resolvers. Wind-off data were obtained several times during the test to evaluate the flexure damping, $L_{\dot{\phi}(f)}$, and roll natural frequency, $\omega_{n(\phi)}$. A summary of the test conditions is presented in Table 2.

IV. Precision of Measurements

The uncertainty in the measurements is a function of the precision of the calibration constants, instrumentation accuracy, repeatability of the flexure characteristics (wind-off data), and the frequency and phase relations. The uncertainties in the dynamic data as a result of the propagation of these errors[4] can be written as follows:

$$\frac{\Delta(L_{\dot{\phi}} + L_{\dot{\beta}} \sin\alpha)}{(L_{\dot{\phi}} + L_{\dot{\beta}} \sin\alpha)} = \left\{(2.00 \times 10^{-4}) + \left[\frac{\Delta L_{\dot{\phi}_f}}{(L_{\dot{\phi}} + L_{\dot{\beta}} \sin\alpha)}\right]^2 + \left(\frac{\Delta\gamma_r}{\tan\gamma}\right)^2\right\}^{1/2}$$

$$\frac{\Delta(L_\beta \sin\alpha)}{L_\beta \sin\alpha} = \left\{(2.50 \times 10^{-5}) + 4\left[\left(\frac{\Delta\omega_{n_\phi}}{\omega_{n_\phi}}\right)\left(\frac{L_{\phi_f}}{L_\beta \sin\alpha}\right)\right]^2\right\}^{1/2}$$

$$\frac{\Delta(N_{\dot{\phi}} + N_{\dot{\beta}} \sin\alpha)}{(N_{\dot{\phi}} + N_{\dot{\beta}} \sin\alpha)} = \left\{(2.00 \times 10^{-4}) + \left[\frac{\Delta N_{\dot{\phi}_f}}{(N_{\dot{\phi}} + N_{\dot{\beta}} \sin\alpha)}\right]^2 + \left[\frac{1}{\tan\Gamma}\left(\Delta\Gamma_r + \frac{N_{\dot{\psi}}\omega}{N_{\dot{\psi}_b}}\right)\right]^2 + 10^{-4}\left[\left(\frac{\omega_{n_\psi}}{\omega}\right)^2 - 1\right]^{-2}\right\}^{1/2}$$

The uncertainty of the calibration constants (0.5%) and instrumentation uncertainties are combined in the first terms of the above equations. The second terms are uncertainties in the flexure characteristics. The third and fourth terms are uncertainties attributable to phase relations and assumptions. The resolver uncertainty is approximately 0.5° ($\Delta\gamma_r = \Delta\Gamma_r = 0.0087$ rad), but during the bench tests system could easily be adjusted to maintained uncertainties within 0.25°.

It is apparent that the most accurate roll-damping data ($L_{\dot{\phi}} + L_{\dot{\beta}} \sin\alpha$) are obtained at the resonant frequency ($\gamma = 90°$), but the precision is not affected significantly if $30 < \gamma < 150$. The uncertainty in the cross derivative ($N_{\dot{\phi}} + N_{\dot{\beta}} \sin\alpha$) can be drastically affected by the phase and frequency relationships. As stated previously, the oscillation frequency, ω, must not be near the natural yaw frequency, and the in-phase yawing moment needs to be minimized (i.e., as the in-phase moment increases, Γ approaches zero) to obtain good data. The yaw-damping term, $N_{\dot{\psi}}\dot{\psi}$, which was omitted in the data reduction equations, is small but may cause an error in the phase relation $N_{\dot{\psi}}\omega / N_{\psi_{(b)}}$ of the same magnitude as $\Delta\Gamma_r$.

Measurement of the tunnel model-support system pitch attitude is precise within 0.05°, based on repeat calibrations. Model attitude corrections were made for balance and sting deflections under air load, and the precision of

Table 3 Data uncertainty

Parameter ( )	Uncertainty			
	Bench tests		Tunnel tests	
	Δ( )/( ) at ( ) = max, %	Δ( ) at ( ) = 0	Δ( )/( ) at ( ) = max, %	Δ( ) at ( ) = 0
$L_{\dot{\phi}} + L_{\dot{\beta}} \sin\alpha$	1.4 at $\gamma = 90$ 5.2 at $\gamma = 5$	0.00008	1.4	0.00020
$L_\beta \sin\alpha$	—	—	2.9	0.25
$N_{\dot{\phi}} + N_{\dot{\beta}} \sin\alpha$	2.0	0.00005	—	—
$Y_{\dot{\phi}} + Y_{\dot{\beta}} \sin\alpha$	2.8	0.00043	—	—
$C_{l_p} + C_{l_{\dot{\beta}}} \sin\alpha$	—	—	1.8	0.0017
$C_{l_{\dot{\beta}}} \sin\alpha$	—	—	3.1	0.00052
C_N	—	—	1.31	0.0028
C_m	—	—	1.02	0.00028

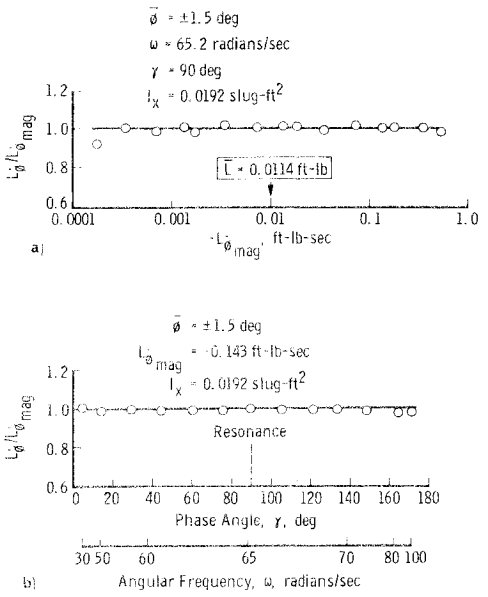

Fig. 4 Comparison of roll-damping measurement to magnetic damper input: a) variation with damping magnitude, b) variation with phase angle and frequency.

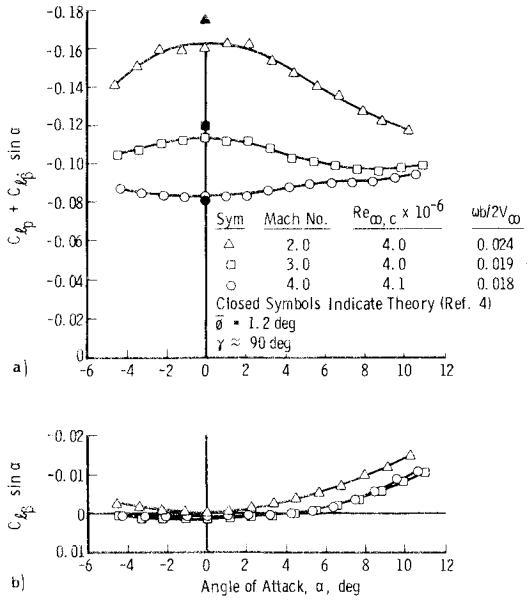

Fig. 6 Variation of roll-damping coefficients with angle of attack and Mach number.

the final model angle-of-attack, α, is estimated to be ±0.07°. The uncertainty in the static balance loads is determined from a statistical analysis of the data obtained during calibration, where loads were applied in each plane and in combination, simulating the range of model loads anticipated for the test.

The preceding uncertainties were combined with uncertainties in the tunnel parameters and expanded using the Taylor series method of error propagation to obtain the probable error in the aerodynamic coefficients. The model used for these tests had a very large I_z to I_x ratio, and the natural yaw and roll frequencies were approximately equal. The model also had a fairly large product of inertia, I_{xz}, because of an unsymmetrical mounting section. Ballast was added to the model to increase I_z in order to separate the natural frequencies ($\omega_{n(\phi)} \approx 1.4\ \omega_{n(\psi)}$), thus permitting the system to obtain roll-damping data; but, because of the large I_{xz} and adverse frequency coupling, the cross-derivative data could not be obtained. The uncertainties in all the parameters are given in Table 3.

V. Results and Discussion

The results obtained in the bench tests are presented in Figs. 4 and 5. The roll-damping measurement shows excellent agreement between the measured value and the magnetic damper input over a large range of damping (Fig. 4a). The uncertainty in the damper is 2% of the input value, which is approximately the same uncertainty which Table 3 gives for the system. At the lower magnitudes the uncertainty of the flexure characteristics be-

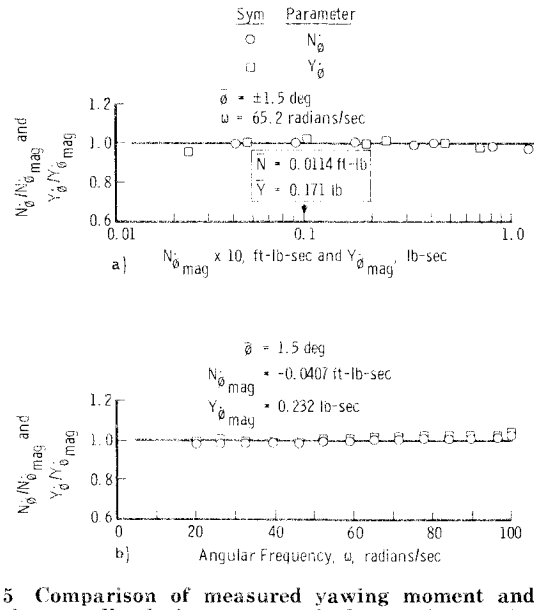

Fig. 5 Comparison of measured yawing moment and side force due to roll velocity to magnetic damper input: a) variation with yawing moment and side force due to roll velocity, b) variation with frequency.

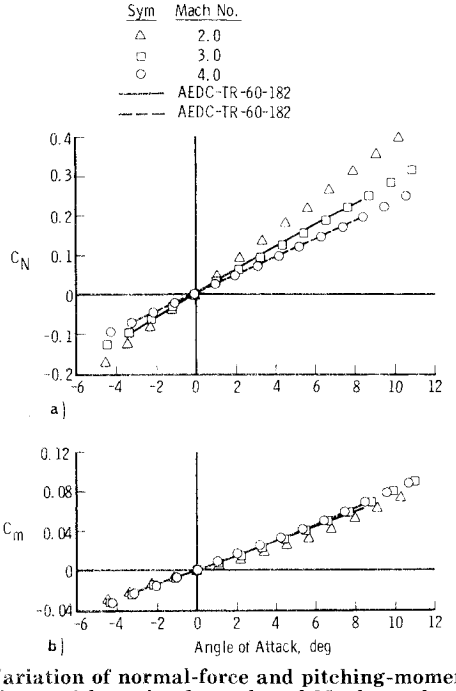

Fig. 7 Variation of normal-force and pitching-moment coefficients with angle of attack and Mach number.

comes the dominant factor. Figure 4b indicates that the resolvers can produce satisfactory results even when the system is operating far off resonance.

Figure 5 shows the results obtained in measuring the yawing moment and side force due to roll velocity produced by the magnetic damper. Excellent agreement was obtained over a large range of yawing moment and side force due to roll velocity (Fig. 5a) and frequencies (Fig. 5b). The slight trend with frequency indicated in Fig. 5b is probably attributable to the uncertainty in obtaining the natural yaw frequency. These data indicate that the cross derivatives $C_{Y(p)}$ and $C_{n(p)}$ can be measured with this system; however, as shown in Sec. III-A and discussed in Sec. IV, model characteristics such as yaw natural frequency and products of inertia are very important in obtaining satisfactory data and must be considered in the model design.

The roll-damping characteristics obtained during the wind tunnel tests on the AGARD Model B are presented in Fig. 6. Only the $Re_{\infty,c} = 4 \times 10^6$ data are presented since no Reynolds number effects were found. The roll-damping coefficient, $C_{l(p)} + C_{l(\dot{\beta})} \sin \alpha$, shows that the model is stable and that the data are symmetrical about $\alpha = 0$ for all Mach numbers, as would be expected. The magnitude of the damping decreases as $|\alpha|$ increases at $M_\infty = 2$ and 3, but the trend is reversed at $M_\infty = 4$. The magnitude of $C_{l(p)} + C_{l(\dot{\beta})} \sin \alpha$ at $\alpha = 0$ decreases as Mach number increases, and the data are in good agreement with theoretical estimates obtained from Ref. 5. The static stability parameter, $C_{l(\beta)} \sin \alpha$, is essentially zero at $\alpha = 0$, and the magnitude increases to produce more stability as $|\alpha|$ increases.

The static coefficients, C_N and C_m, are presented in Fig. 7 as a function of angle of attack, α. C_N increases linearly with α over the range tested, and the slope decreases as Mach number increases. C_m also increases with α, with the Mach 3 and 4 data being at practically the same level, whereas the Mach 2 data increase at a lesser rate. The data are in excellent agreement with data presented in Ref. 6.

VI. Conclusions

A forced-oscillation, dynamic-stability test mechanism was developed for measuring the moments and forces due to roll velocity on lifting configurations. Bench tests and wind tunnel tests on an AGARD Model B were conducted to evaluate the mechanism. Conclusions based on the results of these tests are as follows:

1) The results of the bench tests indicated that the rolling moment, yawing moments, and side force due to roll velocity could be precisely measured by the mechanism.

2) The results of the wind-tunnel tests indicated good agreement between the experimental and theoretical values of the roll-damping coefficient, $C_{l(p)} + C_{l(\dot{\beta})} \sin \alpha$.

3) Yawing moment and side force due to roll velocity could not be obtained in these wind-tunnel tests because of an adverse coupling of the roll and yaw natural frequencies and the large product of inertia, I_{xz}, of this particular model. By careful model design, it will be possible to obtain accurate values of the cross derivatives $C_{Y(p)}$ and $C_{n(p)}$.

References

[1]Orlik-Rückemann, K. J., "Survey of Needs and Capabilities for Wind Tunnel Testing of Dynamic Stability of Aircraft at High Angles of Attack," CR-114583, 1973, NASA.

[2]Schueler, C. J., Ward, L. K., and Hodapp, A. E., Jr., "Techniques for Measurement of Dynamic Stability Derivatives in Ground Test Facilities," AGARDograph 121 (AD669227), Oct. 1967, pp. 23, 61–63.

[3]Welsh, C. J. and Ward, L. K., "Structural Damping in Dynamic Stability Testing," AEDC-TR-59-5 (AD208776), Feb. 1959, Arnold Engineering Development Center, Tullahoma, Tenn.

[4]Beers, Y., *Introduction to the Theory of Error*, Addison-Wesley, Reading, Mass., 1957, pp. 26–36.

[5]Ribner, H. S. and Malvestuto, F. S., Jr., "Stability Derivatives of Triangular Wings at Supersonic Speeds," Rept. 908, 1948, NACA.

[6]Coats, J. D., "Force Tests of an AGARD Calibration Model B at M = 2.5 to 6.0," AEDC-TN-60-182 (AD244544), Oct. 1960, Arnold Engineering Development Center, Tullahoma, Tenn.